JGR Space Physics

RESEARCH ARTICLE
10.1029/2021JA029853

Evidence of Alfvénic Activity in Jupiter's Mid-To-High Latitude Magnetosphere

C. T. S. Lorch[1], L. C. Ray[1], R. J. Wilson[2], F. Bagenal[2], F. Crary[2], P. A. Delamere[3], P. A. Damiano[3], C. E. J. Watt[4,5], and F. Allegrini[6,7]

[1]Space & Plasma Physics Group, Lancaster University, Lancaster, UK, [2]Laboratory for Atmospheric and Space Physics, University of Colorado Boulder, Boulder, CO, USA, [3]Geophysical Institute, University of Alaska Fairbanks, Fairbanks, AK, USA, [4]Department of Meteorology, University of Reading, Reading, UK, [5]Department of Mathematics, Physics and Electrical Engineering, Northumbria University, Newcastle Upon Tyne, UK, [6]Southwest Research Institute, San Antonio, TX, USA, [7]Department of Physics and Astronomy, University of Texas at San Antonio, San Antonio, TX, USA

Key Points:

- New observations of Alfvénic activity in mid-high latitude regions of Jupiter's magnetosphere
- Events are turbulent in nature and are energy dissipative at the electron inertial scale
- Calculated Poynting flux of turbulent perturbations is sufficient to drive auroral emissions

Correspondence to:
C. T. S. Lorch,
c.lorch@lancaster.ac.uk

Citation:
Lorch, C. T. S., Ray, L. C., Wilson, R. J., Bagenal, F., Crary, F., Delamere, P. A., et al. (2022). Evidence of Alfvénic activity in Jupiter's mid-to-high latitude magnetosphere. *Journal of Geophysical Research: Space Physics*, *127*, e2021JA029853. https://doi.org/10.1029/2021JA029853

Received 5 AUG 2021
Accepted 14 MAY 2022

Abstract Using a combination of Juno magnetometer and plasma data, we show evidence of Alfvénic turbulence within the mid-to-high latitude magnetosphere with sufficient conditions to trigger auroral particle acceleration. We analyze 12 events that, in agreement with theoretical results, are found to be dissipative at the electron inertial scale. Furthermore, these events contain significant Poynting flux in the range ~0.8–20 mW/m^2 at ionospheric altitudes. This is sufficient to generate auroral emissions. We confirm that such events are incompressible, confirming their Alfvénicity, occur at dissipative scales, have intermittent features present and are multifractal in nature. These results illustrate the importance of turbulence in the mid-to-high latitudes of Jupiter's magnetosphere as a driver of particle acceleration.

Plain Language Summary Jupiter's aurora is the most powerful in the solar system. Electrons entering the upper atmosphere create these auroral displays, which were originally thought to be generated through a similar mechanism to those at Earth, via semi-stationary electric fields aligned with the magnetic field close to the planet. However the Juno spacecraft in orbit around Jupiter, found much less instances of inverted V electron precipitation (driven by quasi-static potential drops) than expected, therefore other mechanisms are needed along the magnetic field to provide electrons with the necessary energy to enter the planetary atmosphere. Before Juno it was not possible to gather in situ data in these regions. In this paper, we use Juno data to look in these regions for possible acceleration mechanisms and find that turbulence in the magnetic field has the potential to supply the required energy for auroral particle excitation. These results illustrate the importance of magnetic turbulence in Jupiter's space environment.

1. Introduction

The planet Jupiter exhibits unique and striking auroral displays. With emissions 100x more energetic than Earth's, and with a surface brightness up to 10x higher, the Jovian aurora is the brightest and most powerful in the solar system (Clarke et al., 2004). Jupiter's aurora is comprised of three distinguishable components: polar emissions, the main auroral emission (MAE) and satellite footprints. This paper focuses on one potential electron energization mechanisms for the MAE: wave-particle interactions. The MAE is intrinsically linked with the planet's plasma disc, a dense equatorial region of mostly ionized sulfur and oxygen originating from the volcanic moon Io.

A plethora of studies have been carried out using both ground based and in situ measurements to understand the coupling relationship between the generation of MAE and the processes in the plasma disk. Coupling is achieved through field aligned currents, which close in the plasma disk through equatorially flowing currents and in the ionosphere via Pedersen currents. Variations in the structure of the field aligned currents is expected to result in discontinuities and asymmetries in the subsequent MAE (Bonfond et al., 2015; Gustin et al., 2016; Khurana, 2001; Lorch et al., 2020; Radioti et al., 2008). However a number of discrepancies between magnetospheric measurements and auroral observations still remain.

Remote sensing observations provided information on the expected energies required for auroral generation. Spectral observations of FUV aurora from Hubble Space Telescope suggest a mean energy in the range of 30–200 keV for the main auroral emission (Gustin et al., 2004). This compared well with later Hisaki data which identified auroral electron energies to be in the tens to hundreds of keV range (Tao et al., 2016). Prior to the Juno era it was

believed that strong field aligned potentials accelerated electrons to the energies required to precipitate and generate auroral emissions. Magnetospheric electrons were found to have insufficient energy flux of current density in the loss cone to account for the observed auroral emissions (Bagenal et al., 2017; Cowley & Bunce, 2001) and as such required an acceleration mechanism to account for the observations. Work by Ray et al. (2009), in which the terrestrial Knight relation (Knight, 1973) was adapted and applied to Jupiter, showed that parallel potentials of 100 kV are required in order to accelerate electrons to the observed energies. One of the goals of the Juno mission was to identify these field aligned potentials due to its polar orbit, which allows extended detailed measurements over all Jovian latitudes for the first time.

In situ observations by the various instruments on-board Juno have provided a unique insight into the planet's magnetospheric and auroral dynamics. The Waves instrument (Kurth et al., 2017) was used by Louis et al. (2019) to reveal the conjunction between kilometer to decameter wavelength radio emissions and the far ultraviolet wavelength emissions of the MAE, mapping to M-shells between 15 and 60 R_J, where $R_J = 71{,}492$ km is the Jovian equatorial radii. Gérard et al. (2019) presented comparisons between the precipitating electron flux and auroral brightness measurements made during several Juno perijoves. H_2 emission intensities were obtained from the UVS instrument Gladstone et al. (2017), showing the intensity of the main auroral emissions exceeds, matches or falls below the intensity expected from Juno Energetic-particle Detector Instrument (JEDI) measurements. These observations highlight a dependency on the location of the electron acceleration region relative to the spacecraft location, the findings of which were in agreement with theoretical expected acceleration regions. Plasma measurements from JEDI has further revealed the presence of MeV energized electrons over the polar cap and main auroral region (Mauk et al., 2020). Not only have the presence of inverted V structures associated with field aligned potentials been identified in the JEDI data, but also broadband bi-directional electron beams, which were found to be more ubiquitous than the inverted V signatures (Mauk et al., 2017).

At Earth, broadband distributions are associated with electron acceleration in dispersive scale Alfvén waves (e.g., Chaston (2006); Chaston et al. (2002); Wahlund (2003)) where global scale Alfvénic energy is thought to reach dispersive scale lengths via turbulent cascade (Chaston et al., 2008). Similarly, such features at Jupiter can be associated with the effects of propagating dispersive scale Alfvén waves (Damiano et al., 2019; Hess et al., 2010; Watt et al., 2005, 2006) and stochastic wave-particle interactions at dispersive scale lengths (e.g., Allegrini et al. (2017); Saur et al. (2003)). New data from Juno is triggering a re-evaluation of our theories of electron acceleration within the Jovian system (see review of evidence by Bonfond et al. (2020)). It is now understood that dispersive Alfvén wave induced electron acceleration plays a significant part in the generation of the most intense Jovian aurora (Mauk et al., 2017). A later study by Gershman et al. (2019) provided observations of strong Alfvénic turbulence in Jupiter's auroral region during perijove orbits.

The fact that Alfvénic turbulence can feed energy to dispersive scale lengths to facilitate the wave particle interactions that result in the broadband energization is not a new revelation within the Jovian system. Saur et al. (2002) first identified weak MHD turbulence within the plasma disc of the middle magnetosphere. Evidence suggested that dissipation of the weak turbulence was the cause of increasing radial temperature profiles (Ng et al., 2018; Saur, 2004). The interaction between the Jovian ionosphere and magnetodisc results in a transfer of momentum. The decreasing angular momentum of radially moving plasma exerts a stress on the magnetosphere which is balanced by $\mathbf{J} \times \mathbf{B}$ forces in the magnetosphere and ionosphere (Hill, 1979). Saur et al. (2018) stated that for field lines where stress balance is not maintained, Alfvén waves will transfer momentum between the magnetosphere and ionosphere to establish this force balance, interactions between the Alfvén waves and the plasma can lead to stochastic acceleration. The dynamical processes occurring in Jupiter's magnetosphere results in local areas falling out of this pressure balance, allowing such process to occur. Beginning as a disturbance in the magnetospheric plasma by processes such as radial interchange, large scale perturbations propagate along the magnetic field lines and reflect at the ionospheric boundary and the magnetodisc. The reverberating reflections interact non-linearly forming a turbulent cascade which, at small scales, dissipates its energy into the surrounding plasma. In the context of auroral observations, Saur et al. (2003) suggested that the field-aligned potential drop needed to accelerate electrons arises from the coupling of weak MHD turbulence with the global current system. Potentials of 160 kV were estimated to be generated through this process, which is within the range of predictions by Hubble Space Telescope and Hisaki observations.

This estimation was further supported by Clark et al. (2018), who showed that the energies in electron conics observed by Juno/JEDI matched the predictions made by Saur et al. (2003) as well as those of the Knight relation

(Knight, 1973). Clark et al. (2018) also suggested that in order to account for the observed electron energies, it was entirely possible for additional processes to be occurring further along the field line. The existence of turbulence within the magnetodisc (Tao et al., 2016) and at auroral regions has been well documented (Gershman et al., 2019), and extensive work has been done investigating the role of Alfvén waves along field lines threading the satellite footprints (Damiano et al., 2019). However few studies have been undertaken to investigate its presence within the deeper lobe, areas of the magnetosphere adjacent to, but threading, the current disc. This work investigates the presence of one potential acceleration mechanism within this previously unexplored area.

Before the arrival of Juno, Jovian missions were limited in their ability to provide full latitudinal coverage of the system. The Juno spacecraft orbits Jupiter in a polar orbit, with a perijove of $1.05R_J$ and apojove of $113R_J$ (Bolton et al., 2017), where $R_J = 71{,}492$ km is a Jovian radii. The tilt of Jupiter's magnetic axis from its spin axis results in the Juno spacecraft weaving over several magnetic latitudes during a single perijove time frame. The orbital path of the Juno spacecraft makes it an ideal tool to study the variations in Jovian turbulence outside of the equatorial region. This study takes advantage of Juno's unique perspective on the system, which for the first time gives us the opportunity to look for these mechanisms. The JADE-E instrument on-board Juno can detect the variation on electron plasma at the energy levels expected within this region (McComas et al., 2017). JADE coupled with the high-resolution magnetic field instrument (J. Connerney et al., 2017), has the potential to reveal never-before-seen features in the Jovian magnetosphere. The results of this study extends our understanding of turbulence to the mid-high latitude regions of the magnetosphere, revealing some of the additional processes occurring along the field lines threading the auroral region and the magnetodisc.

Our study reveals a sample of Alfvénic activity in the mid-high latitude regions of the Jovian magnetosphere. We define Alfvénic activity as a significant perturbation transverse to the ambient magnetic field. This study initially searched for discrete Alfvénic modes within the magnetosphere. These are assumed to accelerate particles in the mid latitude regions of the magnetosphere where the Alfvén velocity is comparable to the electron thermal velocity, however our search finds evidence of the processes occurring in the mid-to-high latitude regions. In Section 2 we explain the identification and analysis of our events. Section 3 discusses the results and implications toward the global system. We summarize and conclude our findings in Section 4.

2. Identification of Events

Alfvénic activity, manifesting as perturbations in the magnetic field, is expected to generate a parallel electric field at dispersive scale lengths (Lysak & Lotko, 1996). These waves would thus act to accelerate charged particles. Such activity outside of the plasma disk is expected to be small and transient. Larger modes would be reflected at the plasma disk boundaries, while perturbations at smaller scales are able to traverse the field lines outside of the plasma disk (Hess et al., 2010). For this reason, high resolution magnetometer and plasma data is required to observe in detail these structures. Such a level of precision was not available before Juno. The Juno magnetometer instrument has the capacity needed to make such high-resolution measurements, at 64 vector measurements per second, and is in the ideal orbit for our study. This allows a uniquely detailed analysis of the magnetic field within these regions.

Alfvénic perturbations are incompressible with respect to the background field (Alfvén, 1942). It is therefore prudent to identify events using compressional and transverse power spectra of the magnetic field. Spectrograms are produced from high cadence magnetic field data. A Hanning window is applied to limit artificial effects owing to the signal being non-continuous (Eriksson, 2000). The magnetic field is considered in the De Hoffmann-Teller frame of reference (De Hoffmann & Teller, 1950). The De Hoffmann-Teller reference frame is one with the z axis aligned in the direction of the ambient magnetic field, and the x and y axis are perpendicular to the ambient magnetic field. Typically, the y axis is defined as the cross product of the z axis with the relative bulk plasma flow vector. For the scope of this study only the perpendicular component of the perturbation is considered, not the separate x and y components, therefor the x and y vectors are left free to rotate about the z axis. This frame of reference is chosen as to ascertain perturbations parallel and perpendicular to the background field. This is key to providing evidence of Alfvén wave activity, which is expected to exhibit a perturbation transverse to the magnetic field. To rotate into this frame we identify the background field using a 120s rolling average. A window of 120s was chosen as it is sufficiently large to capture the relatively slow variation of the magnetic field when compared with the variations of the perturbed field. Periods where the total transverse power undergoes a significant

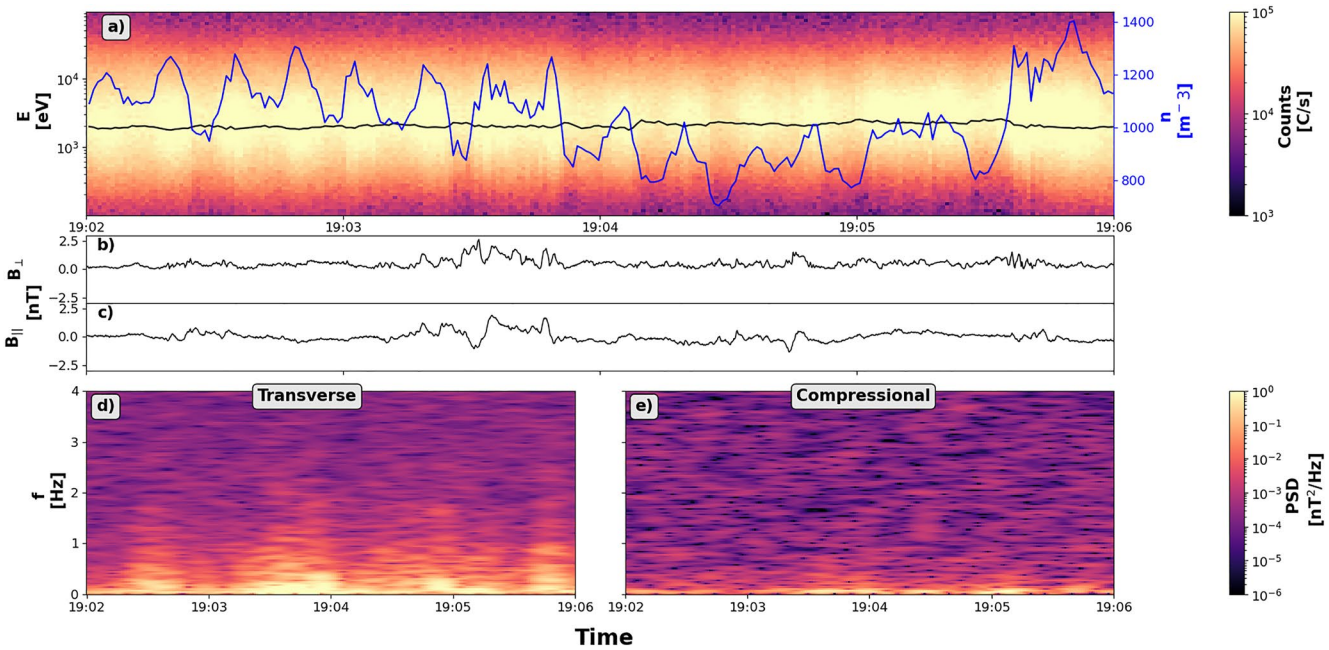

Figure 1. Electron plasma and magnetic field data in the dawn sector for a period during 2017-138. Panel (a) shows the high resolution JADE-E electron plasma data. The temperature (black profile) and number density (blue profile) calculated from the plasma moments are overlaid. Panels (b) and (c) show the perpendicular and parallel components of the magnetic field in the De Hoffmann-Teller reference frame. A detrending procedure was implemented in order to highlight the transient perturbations in the field. Panels (e) and (f) show the power spectra of the transverse and compressional field respectively. Compressional signals appear absent from the event, while a clear, broad increase in transverse power indicates the presence of Alfvénic turbulence.

increase above the background level, in conjunction with significant field perturbations, are recorded. Figure 1 shows an example of one event used in this study at date 2017-138. Figures 1a and 1b have been detrended by subtraction of the 120s background average in order to highlight the transient perturbations. As the spectral power is prominent in the transverse component and not in the compressional component, see Figures 1d and 1e, it may be deduced that these perturbations are Alfvénic in nature. Furthermore, broad increases in power over a range of frequencies is indicative of Alfvénic turbulence rather than discrete modes. This might be expected, as the reverberations of reflected Alfvén waves would interact non-linearly to form a turbulent structure.

It is necessary to characterize the length scales associated with turbulent features in order to discern possible energy dissipation mechanisms. The JADE plasma instrument on board Juno can provide the plasma parameters required to calculate these scales accurately. For the regions within which the events are located, interactions are expected to occur at the electron plasma scale (Saur et al., 2018). In this study, high resolution data from the JADE-E instrument was used to obtain information about the local plasma population during transient events. In order to resolve temporally short events, Nyquist sampling theorem requires the resolution of comparable data to be at least half the duration of the observed event. For this reason, event selection is restricted to regions where the JADE-E plasma instrument is at its highest cadence.

Utilizing this search method multiple potential events were identified. The events most comparable to Alfvénic activity were found in the mid-high latitudes, over 60°, with latitudes below this tending toward MHD turbulence containing compressional components. A subset of 12 events, which coincided with times where high resolution plasma data was available, were chosen for this study. These events are spaced out over several orbits but are constrained to the dawn sector. The 12 events are quasi-discrete. Some events consist of individual perturbations spanning a few minutes while others exhibit several concurrent disturbances in the field. The distribution of the events used in this study can be seen in Figure 2, Table 1

Table 1
The Time, Duration, M-Shell Mapping and Jupiter Solar Magnetic Coordinates of the 12 Events Identified in This Study

Event	Start time [UT]	Duration [s]	M-shell [R_J]	JSM (X,Y,Z) [R_J]
1	2017-05-18 19:02:00	239	39.48	(−4.51, −10.40, 4.44)
2	2017-05-18 19:06:00	1019	33.41	(−4.49, −10.38, 4.37)
3	2017-05-18 19:24:00	359	23.82	(−4.39, −10.28, 4.05)
4	2017-05-19 12:13:00	149	45.89	(−1.51, −5.95, −5.33)
5	2017-05-19 12:55:00	179	46.96	(−1.72, −6.44, −5.70)
6	2017-07-10 17:03:00	359	25.59	(−4.50, −8.29, 4.55])
7	2017-07-10 17:10:00	239	23.28	(−4.46, −8.26, 4.44)
8	2017-07-10 17:15:00	239	21.73	(−4.43, −8.23, 4.36)
9	2017-09-01 12:18:00	419	32.01	(−5.44, −7.89, 5.43)
10	2017-09-01 12:30:00	899	31.95	(−5.36, −7.69, 5.47)
11	2017-09-01 14:13:00	239	26.14	(−4.57, −6.48, 5.04)
12	2017-09-01 14:29:00	239	24.01	(−4.45, −6.36, 4.87)

3. Energy Regime of Turbulent Events

The initial search into identifying Alfvénic activity within the Jovian system yielded results that suggest the presence of Alfvénic turbulence rather than that of discrete wave-forms. Following the well-established work by von Papen et al. (2014) and Tao et al. (2015), a wavelet analysis technique was applied to reveal the nature of the perturbations. The wavelet transform allows us to calculate the power spectral density of our events. The transform, $W_i(t, \tau)$ is given as

$$W_i(t,\tau) = \Sigma_{j=1}^{N} B_i(t_j) \frac{1}{\sqrt{\tau}} \psi^* \left[\frac{(t_j - t)}{\tau}\right] \Delta t \tag{1}$$

where N is the length of the time array, B_i is a component of the detrended magnetic field signal, t_j indicates the time index, while τ is the inverse of the frequency and Δt is the time increment between measurements. ψ^* is the complex conjugate of the Morlet wavelet, defined by

$$\psi(x) = \pi^{-\frac{1}{4}} e^{i\omega_0 x - \frac{x^2}{2}} \tag{2}$$

where $\omega_0 = 6$. The results of a wavelet analysis for one event is shown in Figure 3, where panel a) represents the parallel component, $W_{\parallel}$, and panel b) is the perpendicular component, $W_{\perp}$. $W_{\parallel}$ shows little variation over the course of the event. However $W_{\perp}$ exhibits a repeating increase in the power spectra over mid range frequencies. Again, a perpendicular power increase over a broad range of frequencies, such as those occurring between 19:03 - 19:04, is observed supporting the hypothesis that this event is an example of Alfvénic turbulence.

The results from the wavelet analysis are then used to calculate the the power spectral density for the event with:

$$PSD_i(\tau) = \frac{2}{N\Delta t} \Sigma_{j=1}^{N} \Delta t |W_i(t_j, \tau)|^2 \tag{3}$$

In a turbulent system, large scale structures undergo a cascade to smaller and smaller scales, during this cascade energy can either enter or leave the system. The change in power spectral density with respect to frequency can be determined through fitting a power law to the given spectra. This provides information on how the energy within the turbulent system is changing. The point at which the power spectra gradient changes abruptly is referred to as the spectral break. The frequency at which the spectral break occurs can provide information on how energy is being gained or lost from the cascade.

In order to ascertain the power law, and subsequent spectral break, associated with the perturbations in this study an optimized fitting routine was applied with a sliding window to the spectral profiles. The frequency range over which the spectral index was steepest was determined by the sliding fit routine. Spectral indices between −1.87

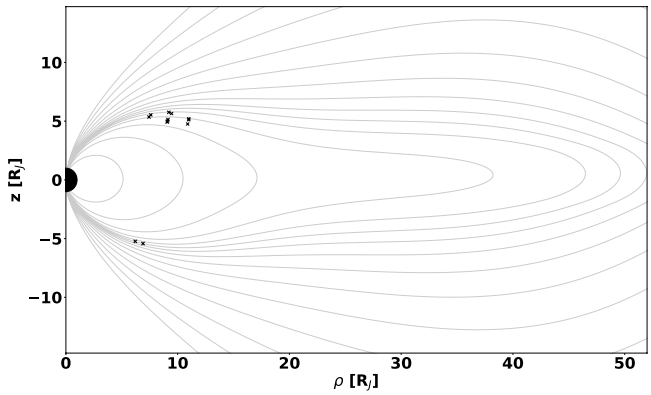

Figure 2. The location of the 12 identified events in the magnetic frame of reference. Events are localized in the mid-to-high latitude regions, mapping to equatorial radii, or M shells, between 20 and 50 R_J, conjugate with the main auroral emissions. Mapping was performed using the JRM09 magnetic field (J. E. P. Connerney et al., 2018) and CAN current disc (J. E. P. Connerney, 1981) models. Events used in this study are all within the dawn sector.

and −2.71, representing a dispersive turbulent regime (Leamon et al., 1999), were found to fit the profiles at the higher frequency range, approximately between 0.1 and 6 Hz. This shows that for all events, there is potential for energy dissipation at scales within the high frequency range. Lower frequency gradients were found by fitting a straight line to the profile between the lower frequency cut off and the start of the higher frequency gradient. Power laws in these ranges were much shallower, corresponding to an energy-containing scale (Goldstein et al., 1995). The fitting algorithm was not used here as the spectral break in the spectral profile had been located. The black lines in Figure 4 show the fitted power laws before and after the spectral break.

The Alfvénicity, how Alfvénic an event is, can now be checked by calculating the compressibility of the event. This is given by the ratio of the parallel PSD component over the total PSD, $\frac{PSD_{\parallel}}{PSD_{total}}$. Events with an isotropic power distribution would have a compressibility ratio of 0.33. Likewise, for a fully compressional signal we would expect a value of 1. Events with a low compressibility are more Alfvénic in nature, hence this method provides a way of confirming the initial assumption that the events are Alfvénic. Figure 5 shows the compressibility of all events. The frequency axis has been normalized by the spectral break frequency, providing a clear illustration that frequencies within the dissipative regime have a low compressibility.

Events in this study lie largely below the isotropic value, denoted by the horizontal dashed black line, for low to mid range frequencies. The maroon profile represents the binned median value of the events, with error bars indicating the median absolute deviation calculated by

$$MAD = Median\left(|X_i - \tilde{X}|\right) \tag{4}$$

where X_i is each respective value of the bin and $\tilde{X}$ is the bin's median value. This trends asymptotically toward an isotropic distribution at higher relative frequencies. This result confirms the assumption that events are Alfvénic in nature. With this information it is then possible to estimate the Poynting flux of the events without knowledge of the electric field.

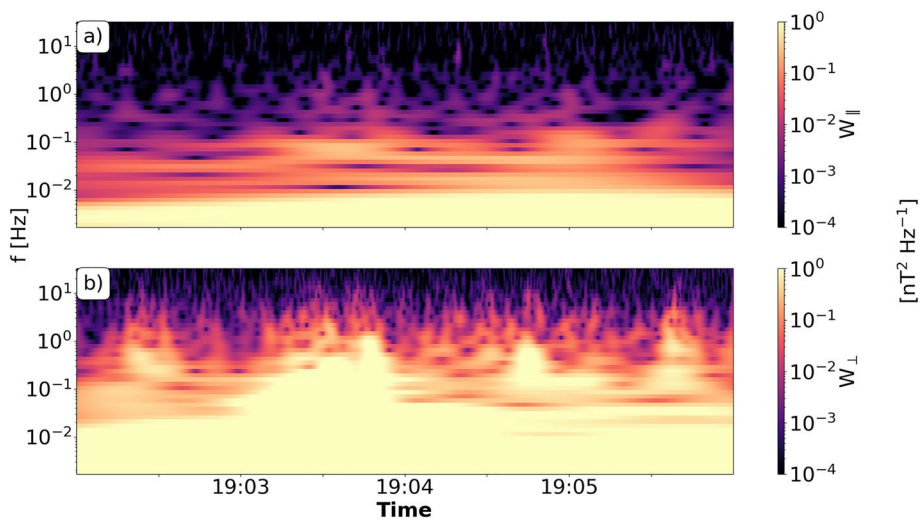

Figure 3. The results of the wavelet analysis from event during 2017-138 in the dawn sector. (a) The parallel component of the power spectra. (b) the perpendicular component of the power spectra.

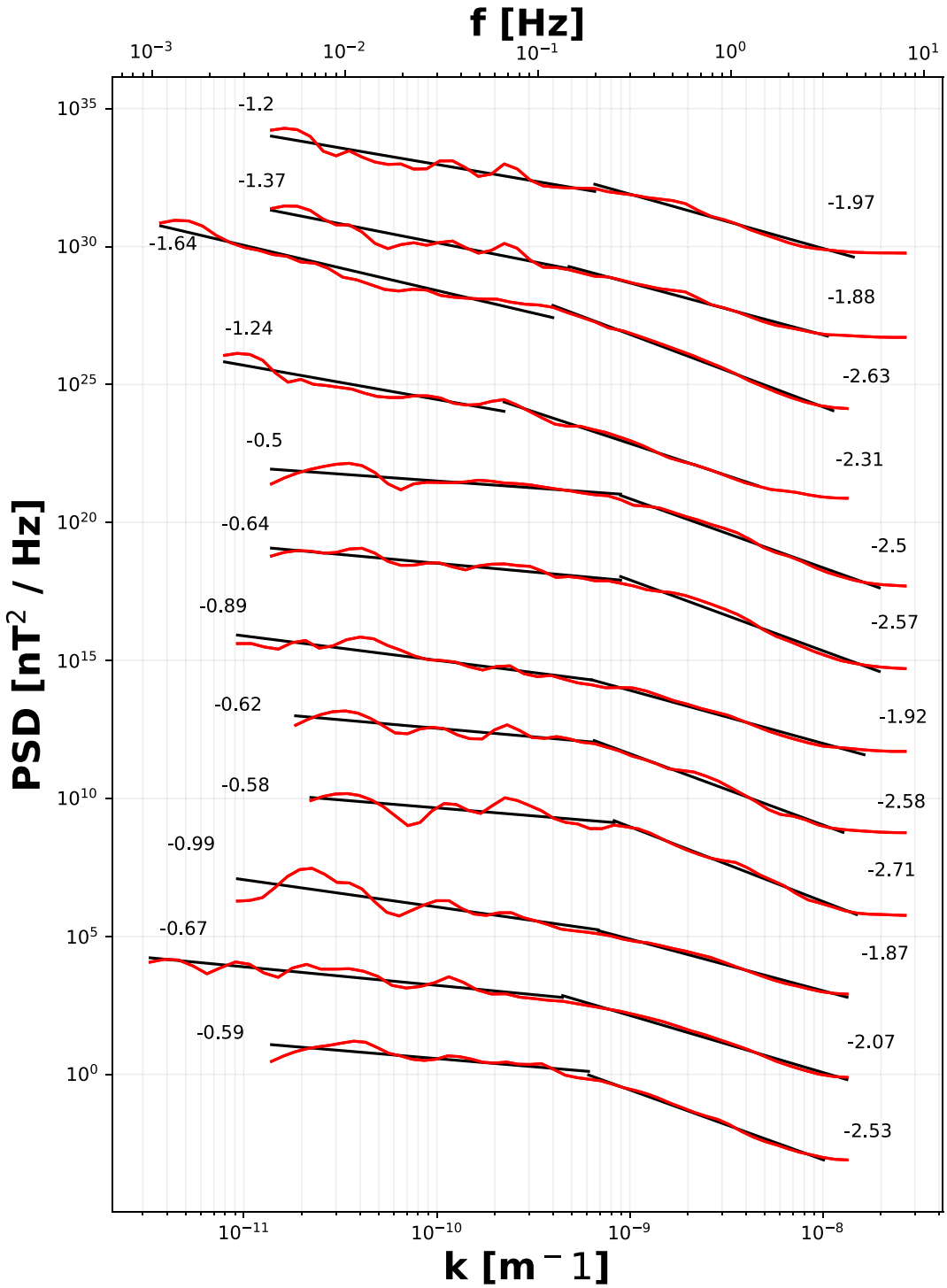

Figure 4. The calculated power spectral densities of each event. The PSD of each event, show in red, are scaled by 10^{3n} where n is the number of the event. Scaling was used to aid visualization. Black lines indicate the fitted power laws. The higher frequency power laws were fitted using the devised optimisation technique, while lower frequency gradients were fitted between the event specific lower frequency cut off and the higher frequency spectral break. The fitted power laws can all be seen to transition from a non-dispersive regime at lower frequencies to a dispersive, and potentially dissipative, regime at higher frequencies.

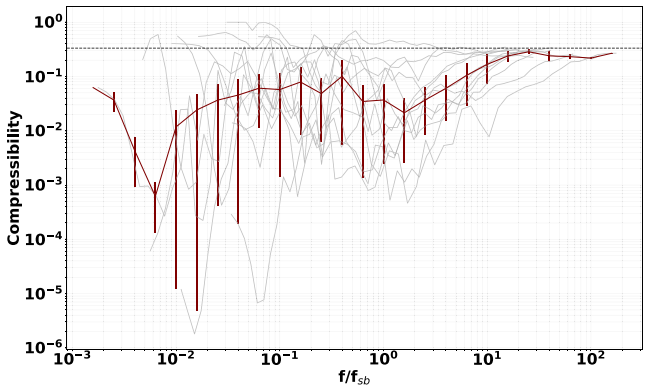

Figure 5. The compressibility of each event, represented by light gray lines, over frequency. The frequency has been normalized based off the spectral break in each event to highlight the compressibility within the energy dissipative regions. The black horizontal line marks the value expected for power isotropy. Values above this line indicate a more compressible signal, while values below it are more incompressible. The maroon profile represents the binned median value of each event, with error bars denoting the median absolute deviation.

4. Discussion and Interpretation

4.1. Poynting Flux

A key comparison which can be made between these results and auroral observations is the Poynting flux. Sufficient Poynting flux can provide the energy which drives auroral particle precipitation and comparisons with observed values can indicate whether these events might result in auroral emissions. Usually this would require knowledge of the electric field, however by confirming the events are indeed Alfvénic in nature, the associated Poynting flux can instead be calculated purely with knowledge of the magnetic field:

$$S = \frac{(\delta B_{bp})^2 c}{\mu_0} \quad (5)$$

For a more suitable calculation of the Poynting flux, δB_{bp} is the root mean square of the amplitude of the magnetic perturbations. This was calculated using a 5th order Butterworth band pass filter (Prêle, 2017). The filter has frequency cut-offs set at the upper and lower boundary of the optimized power law fit. The resultant varience was summed and the square root taken to give δB_{bp}. The values of δB_{bp} and the resultant localized Poynting flux are shown in Table 2.

This initial calculation returns the localized Poynting flux. To compare with auroral energy fluxes the result must be scaled to ionospheric altitudes. Assuming the perturbations are confined to an individual flux tube the area of said flux tube would be expected to scale with the mirror ratio. Using the JRM09 magnetic field model (J. Connerney et al., 2017) a magnetic field trace is made to the ionosphere (altitude of 1.1RJ) and a local mirror ratio is returned. By simply multiplying the local Poynting flux with the returned mirror ratio an estimation of the scaled Poynting flux is produced. These results are presented in the fourth column of Table 2.

In Gustin et al. (2016) mean auroral energy fluxes of 100 mW/m^2 were found to be sufficient in order to excite high intensity FUV emissions, while Saur et al. (2003) calculated an energy flux of 7 mW/m^2 corresponding to the region of maximum turbulent power at 20R$_J$. More recent estimates by Saur et al. (2018) place this value around 6 mW/m^2, which correspond to 100 mW/m^2 at auroral altitudes. Auroral altitude Poynting flux from the events in this study are comparable to energy flux values observed by Gustin et al. (2016), and are within the 8 – 280 mW/m^2 range measured by JEDI (Mauk et al., 2017, 2018). Assuming a dissipation efficiency of 10% (Hess et al., 2010) the scaled calculations of the Poynting flux are comparable to this value implying the events shown here have sufficient Poynting flux to generate auroral emissions. However, Gershman et al. (2019) found no traces of Alfvénic perturbations at perijoves over the main auroral emission. This might suggest that the turbulent fluctuations were reflected by the higher density gradients in the plasma disk before they reached these altitudes and as such turbulent energy within these latitudes contribute to magnetospheric plasma heating rather than auroral electron acceleration.

Table 2
A Summary of the Events Poynting Flux

Event	δB [nT]	S_{local} [μW/m^2]	$S_{1.1R_J}$[mW/m^2]
1	0.312	23.2	51.4
2	0.281	18.8	40.7
3	0.179	7.66	15.0
4	0.440	46.2	37.1
5	0.361	31.1	30.2
6	0.186	8.24	11.8
7	0.406	39.3	54.7
8	0.384	35.3	47.5
9	0.319	24.3	47.8
10	0.675	109	196
11	0.160	6.14	6.84
12	0.181	7.85	7.97

Note. Given for each event are the field perturbation, local and low altitude Poynting flux. The perturbed field was calculated as the sum of the variance of the band filtered magnetic field. The Poynting flux was scaled to ionospheric values by use of a mirror ratio calculated with the JRM09 magnetic field model.

4.2. Turbulent Scales

As discussed in Section 2, the power law associated with the power spectra indicates that at higher frequencies the turbulent perturbations are within the energy dissipative regime. Within this regime, energy can be lost to the environment, in this case the surrounding plasma. Dissipation of energy occurs in the form of dampening and heating of the surrounding plasma, the mechanism through which this occurs is determined by the scale of the turbulent perturbations. For the events in this study, the dissipation mechanism can

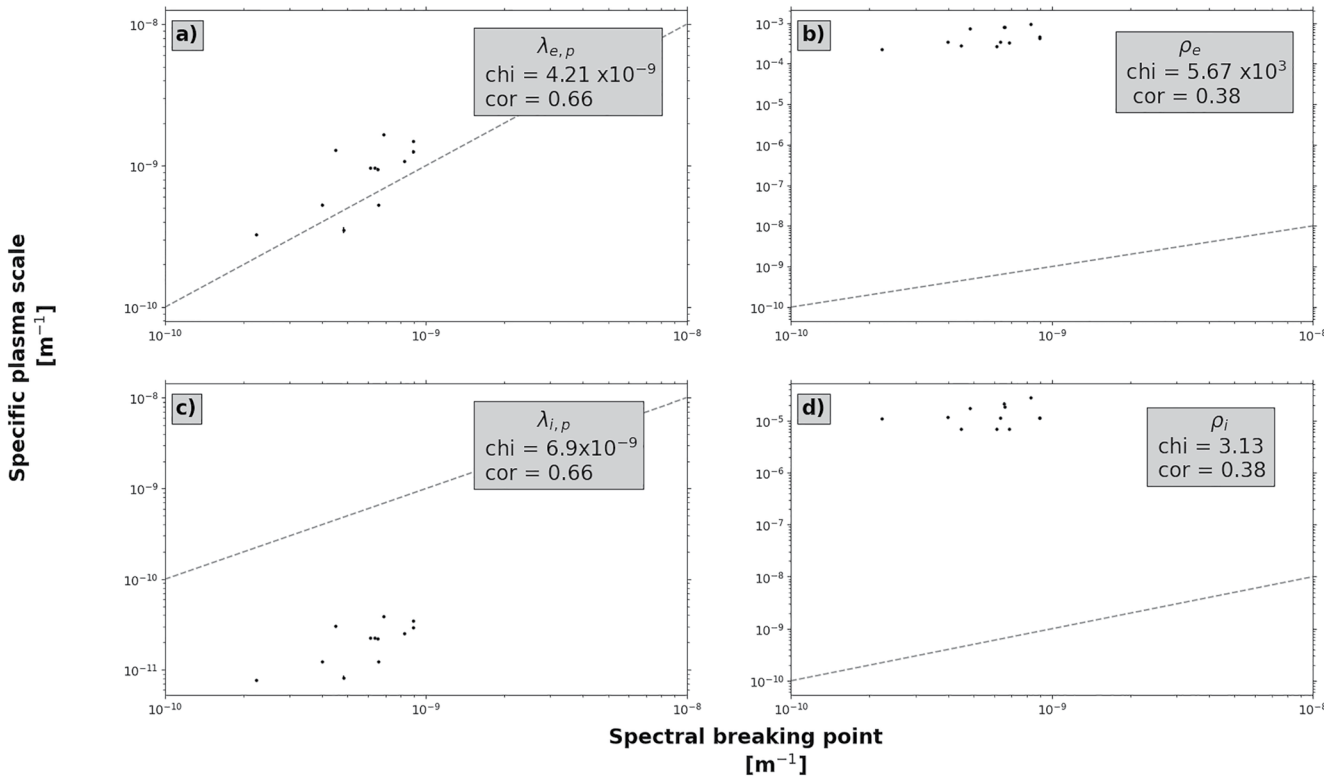

Figure 6. A comparison between the spectral breaking length scale and fundamental plasma lengths. (a) Electron inertial length: $\frac{c}{\omega_{p,e}}$, (b) electron gyro radius: $\frac{m_e v_\perp}{|q|B}$, (c) ion inertial length $\frac{c}{\omega_{p,i}}$ and (d) ion gyro radius: $\frac{m_i v_\perp}{|q|B}$. The χ^2 fit and correlation coefficient for each comparison are included in the upper right section of each panel. Error bars included here represent twice the standard error of the mean.

be discerned through comparisons of fundamental plasma length scale with the spectral break length scale. Within these regions of the magnetosphere a semi-relativistic approach must be considered in order to discern the respective length scales of the turbulent events (Gershman et al., 2019). Utilizing the dispersion relation for semi-relativistic Alfvén waves, transformation between the frequency and length scales can be achieved. The respective dispersion relation is:

$$\omega = v_A k \cos(\theta) \approx c k_{\parallel} \tag{6}$$

For comparisons between the spectral break frequency and the fundamental length of the plasma it was necessary to utilize high resolution JADE-E instrument. JADE-E enabled us to obtain plasma parameters during the transient perturbations in the magnetic field. Providing a greater level of understanding of the events than model estimates alone. Assuming an isotropic distribution the plasma moments were calculated and used to obtain the respective frequencies.

Figure 6 shows the comparison of several fundamental inverse plasma scales with the inverse spectral break length scale obtained through the optimisation algorithm. These correspond to length scales between 16 and 70 R_J. The dashed line here indicates unity. A χ^2 fitting and correlation analysis were used to quantify the closest fit. The lower the χ^2 value, the closer the calculated scales are to the spectral break point, while the closer the correlation value is to 1, the higher the correlation between the two frequencies. The closest fit can be seen to be with the electron plasma scales, or electron inertial length. This suggests that energy from the turbulent fluctuations can be lost to electrons at this scale. It has been suggested by many sources that Alfven wave energy would be dissipated at electron inertial scales, or skin depth, at high latitudes through wave particle interactions (e.g., Chaston et al. (2002); Damiano et al. (2019); Hess et al. (2010); Lysak & Lotko (1996); Saur et al. (2003); Watt et al. (2005, 2006)). As can be seen in Figure 6, the scale closest to the spectral break is indeed the electron inertial scale. The dissipative turbulent scales measured for these events is in agreement with theoretical scale predictions by Saur et al. (2018) for the same region.

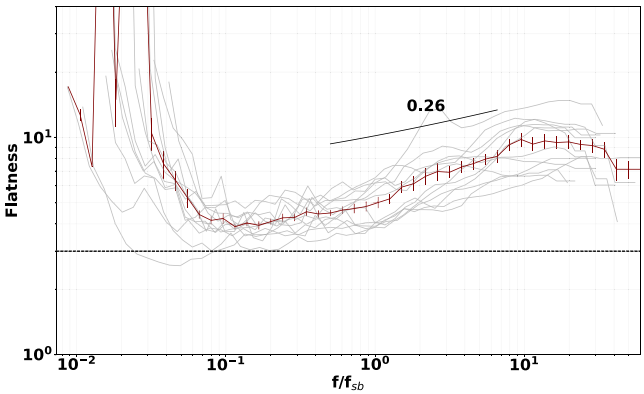

Figure 7. The flatness of each event normalized by the spectral break frequency of each event. The maroon profile indicates the mean flatness value, with error bars expressing the standard error of the mean. A dashed horizontal line represents a flatness of 3, for a Gaussian distribution. The large values toward the low frequency end are due to boundary effects, while the decrease at high frequencies is due to the instrument sampling boundary. The gradient fit over higher frequency ranges, with a positive value of 0.26, suggests that the turbulent events are multifractal in nature.

4.3. Intermittency

Turbulence must undergo a cascade from larger to smaller scales in order to facilitate energy transfers. In order to support the hypothesis that events in this study could lose energy to the surrounding plasma it is necessary to look for evidence of this cascade. Perturbations undergoing such a cascade would be expected to exhibit intermittency, seen as tails in probability density functions of the time lagged magnetic field (Carter, 2006), which have been associated with the presence of coherent structures in other studies (Meyrand et al., 2015; Veltri, 1999). A coherent structure is the term given to the relatively ordered structures within a turbulent flow, such as vorticies, which are concurrent with a turbulent cascade (Fazle Hussain, 1986). The time lagged magnetic field, δB_t, is given by

$$\delta B_{i,t}(t,\tau) = \delta B_i(t+\tau) - \delta B_i \tag{7}$$

where τ is a time period consistent with the frequencies used in the wavelet analysis. Tails in the probability density function can be quantified by calculating the flatness or kurtosis of the function. This is carried out using structure functions of the 2^{nd} and 4^{th} order, $F_i(\tau) = \frac{\xi_i^4(\tau)}{|\xi_i^2(\tau)|^2}$. The mth order structure function is given as:

$$\xi_i^m(\tau) = \frac{1}{N}\Sigma_{j=1}^{N}|\delta B_{i,t}(t_j,\tau)|^m \tag{8}$$

In the case of a Gaussian probability density function the corresponding flatness would be $F_i(\tau) = 3$. As such, a flatness of 3 would suggest there is no intermittency in the events and no energy transfers would be facilitated. Any values over this threshold suggests that intermittency is indeed present, that the events are undergoing a cascade and energy transfers are likely to occur.

For each event the mean flatness of the three components is taken to be the flatness of the probability density function, this is shown in Figure 7. Note that again, the frequency has been normalized by the spectral break frequency to aid in comparison. As can be seen in Figure 7, the flatness of the events, over dissipative frequencies, are greater than that of a Gaussian profile. This demonstrates the presence of intermittency, and hence the presence of a turbulent cascade which would dissipate energy to the surrounding plasma. This would also suggest that the turbulent cascade is facilitated outside of the magnetodisc at higher latitudes. Counter propagating Alfvén waves would be expected in the mid-to-high latitude regions as Alfvén wave reflections would likely occur where $\frac{B}{n}$ has a maximum at higher latitudes and at the magnetodisc boundary in the lower latitudes.

Analysis of turbulence in these mid-to-high latitude regions has not been done previously. However Tao et al. (2015) determined the nature of turbulence within the plasma disc and the lobe region beside the plasma disc boundary. They find large flatness values within the plasma disc, with high frequency values increasing exponentially reaching 100 at the upper cut-off, suggesting a strongly intermittent turbulence. Their lobe region values however, peak around the mid frequency range at a value of around 4, before settling at a Gaussian flatness value of 3 at the higher frequencies. This would indicate the noise floor of the instrument has been reached. The increasing gradient of the mean flatness indicates multifractal behavior (Jiménez, 2006).

The results found from this analysis are betwixt those of the plasma disc and lobe regions discussed in Tao et al. (2015), indicating the presence of intermittency within the turbulent regions, but not as strong as that found in the plasma disc.

5. Summary

Using high resolution Juno magnetometer and plasma data Alfvénic activity within the mid-to-high latitudes of Jovian magnetosphere is investigated. 12 events of interest were identified on field lines magnetically conjugate with Jupiter's main auroral emission and where both magnetometer data and plasma data were available at the

desired resolution. These events provide a glimpse of a very dynamic system where turbulence and wave-particle interaction are energizing the local plasma. Our key findings are:

1. Alfvénic turbulence exists in the mid-to-high latitude region of Jupiter's magnetosphere on field lines magnetically conjugate with the main auroral emission.
2. Wavelet analysis shows that the power spectral density of these events and associated power laws (−1.87 to −2.71) are consistent with turbulence in the energy dissipative regime.
3. PSD profiles in Figure 4 are show to exhibit spectral breaks at frequencies approaching the electron plasma frequency ($0.06 \leq \omega_{e,p} \leq 0.3$ Hz) in Figure 6. Fundamental frequencies were calculated from JADE-E plasma moments. This suggested that turbulent energy is dissipated into the local electron population and is in agreement with previous theoretical work (Saur et al., 2018).
4. Applying a Butterworth band pass filter over the magnetic field signal between dissipative frequencies, we estimate the Poynting flux and scale to the ionosphere. Our ionospheric values are comparable to those inferred from auroral observation and match well with predicted energy fluxes associated with turbulent acceleration of magnetospheric electrons (e.g., Saur et al. (2003)).
5. Analysis of the perturbed field indicates the presence of intermittency, a feature common in processes undergoing a turbulent cascade. The variation in probability density flatness with frequency points toward turbulence of a multi-fractal nature.

These key findings paint an interesting picture. Alfvénic turbulence has the potential to energize electrons within regions of the magnetosphere outside the expected acceleration region for quasi-static electric fields. Future work should aim to systematically investigate and quantify the global variations in both Alfvénic and MHD turbulence within the Jovian magnetosphere. Juno's exploration of non-equatorial latitudes offers the prime opportunity to carry out this investigation.

Data Availability Statement

Juno data used in this work was retrieved from the Planetary Data System (PDS) database (https://pds-ppi.igpp.ucla.edu/). The magnetometer data was from dataset JNO-J-3-FGM-CAL-V1.0 (https://doi.org/10.17189/1519711), utilizing the fgm_jno_l3_yyyydddpc_v01.sts files and fgm_jno_l3_yyyydddpc_v02.sts files toward perijove. JADE-E data was obtained from dataset JNO-J/SW-JAD-3-CALIBRATED-V1.0 (https://doi.org/10.17189/1519715), using the high-rate science electron data files JAD_L30_HRS_ELC_TWO_CNT_yyyyddd_V02.DAT and JAD_L30_HRS_ELC_TWO_CNT_yyyyddd_V03.DAT.

Acknowledgments
C.T.S. Lorch was funded by an STFC Studentship. L.C. Ray was funded by STFC Consolidated Grant ST/R000816/1 to Lancaster University. This work was supported by F. Bagenal and R.J. Wilson at the University of Colorado as a part NASA's Juno mission supported by NASA through contract 699050X with the Southwest Research Institute. P.A. Delamere was supported under the NASA grant NASA/80NSSC20K1279. P.A. Damiano was supported by NASA grant 80NSSC19K094. C.E.J. Watt was supported by STFC grants ST/W002078/1 and ST/W000369/1. The authors offer their thanks to the editor and reviewers who provided feedback on this work and helped craft it into its final form.

References

Alfvén, H. (1942). Existence of electromagnetic-hydrodynamic waves. *Nature*, *150*(3805), 405–406. https://doi.org/10.1038/150405d0

Allegrini, F., Bagenal, F., Bolton, S., Connerney, J., Clark, G., Ebert, R., et al. (2017). Electron beams and loss cones in the auroral regions of Jupiter. *Geophysical Research Letters*, *44*, 7131–7139. https://doi.org/10.1002/2017GL073180

Bagenal, F., Adriani, A., Allegrini, F., Bolton, S., Bonfond, B., Bunce, E., et al. (2017). Magnetospheric science objectives of the Juno Mission. *Space Science Reviews*, *213*, 219–287. https://doi.org/10.1007/s11214-014-0036-8

Bolton, S., Lunine, J., Stevenson, D., Connerney, J., Levin, S., Owen, T., et al. (2017). The Juno Mission. *Space Science Reviews*, *213*, 5–37. https://doi.org/10.1007/s11214-017-0429-6

Bonfond, B., Gustin, J., Gérard, J.-C., Grodent, D. S., Radioti, A., Palmaerts, B., et al. (2015). The far-ultraviolet main auroral emission at Jupiter - Part 1: Dawn-dusk brightness asymmetries. *Annales Geophysicae*, *33*, 1203–1209. https://doi.org/10.5194/angeo-33-1203-2015

Bonfond, B., Yao, Z., & Grodent, D. (2020). Six pieces of evidence against the corotation enforcement theory to explain the main aurora at Jupiter. *Journal of Geophysical Research: Space Physics*, *125*(11). https://doi.org/10.1029/2020JA028152

Carter, T. (2006). Intermittent turbulence and turbulent structures in a linear magnetized plasma. *Physics of Plasmas*, *13*, 010701. https://doi.org/10.1063/1.2158929

Chaston, C. (2006). ULF waves and auroral electrons. In K. Takahashi, P. Chi, R. Denton, & R. Lysak (Eds.), *Magnetospheric ulf waves: Synthesis and new directions* (pp. 239–257). Geophysical Monograph Series 169. https://doi.org/10.1029/169GM16

Chaston, C., Bonnell, J., Peticolas, L., Carlson, C., McFadden, J., & Ergun, R. (2002). Driven Alfvén waves and electron acceleration: A FAST case study. *Geophysical Research Letters*, *29*(1535). https://doi.org/10.1029/2001GL013842

Chaston, C., Salem, C., Bonnell, J., Carlson, C., Ergun, R., Strangeway, R., & McFadden, J. (2008). The Turbulent Alfvénic Aurora. *Physical Review Letters*, *100*(17), 175003. https://doi.org/10.1103/PhysRevLett.100.175003

Clark, G., Tao, C., Mauk, B., Nichols, J., Saur, J., Bunce, E., et al. (2018). Precipitating electron energy flux and characersitic energies in Jupiter's main auroral region as measured by Juno/JEDI. *Journal of Geophysical Research: Space Physics*, *123*, 7554–7567. https://doi.org/10.1029/2018JA025639

Clarke, J., Grodent, D., Cowley, S., Bunce, E., Zarka, P., Connerney, J., & Satoh, T. (2004). Jupiter's Aurora. In F. Bagenal, T. Dowling, & W. McKinnon (Eds.), *Jupiter the planet, satellites and magnetosphere* (pp. 639–670). Cambridge University Press.

Connerney, J., Benn, M., Bjarno, J., Denver, T., Espley, J., Jorgensen, J., et al. (2017). The juno magnetic field investigation. *Space Science Reviews*, *213*, 39–138. https://doi.org/10.1007/s11214-017-0334-z

Connerney, J. E. P. (1981). The magnetic field of Jupiter: A generalized inverse approach. *Journal of Geophysical Research*, *86*, 7679–7693. https://doi.org/10.1029/ja086ia09p07679

Connerney, J. E. P., Kotsiaros, S., Oliversen, R. J., Espley, J. R., Joergensen, J. L., Joergensen, P. S., et al. (2018). A new model of Jupiter's magnetic field from Juno's first nine orbits. *Geophysical Research Letters*, *45*, 2590–2596. https://doi.org/10.1002/2018GL077312

Cowley, S., & Bunce, E. (2001). Origin of the main auroral oval in Jupiter's coupled magnetosphere–ionosphere system. *Planetary and Space Science*, *49*(10), 1067–1088. https://doi.org/10.1016/S0032-0633(00)00167-7

Damiano, P., Delamere, P., Stauffer, B., Ng, C.-S., & Johnson, J. (2019). Kinetic simulations of electron acceleration by dispersive scale Alfvén Waves in Jupiter's Magnetosphere. *Geophysical Research Letters*, *46*, 3043–3051. https://doi.org/10.1029/2018GL081219

De Hoffmann, F., & Teller, E. (1950). Magneto-hydrodynamic shocks. *Physical Review*, *80*(4), 692–703. https://doi.org/10.1103/PhysRev.80.692

Eriksson, A. (2000). Spectral analysis. In G. Paschmann, & P. Daly (Eds.), *Analysis methods for multi-spacecraft data* (pp. 5–42). ESA Publications Division, KeplerlaanISSI Scientific. Report SR-001.

Fazle Hussain, A. (1986). Coherent structures and turbulence. *Journal of Fluid Mechanics*, *173*, 303–356. https://doi.org/10.1017/S0022112086001192

Gérard, J.-C., Bonfond, B., Mauk, B., Gladstone, G., Yao, Z., Greathourse, T., et al. (2019). Contemporaneous observations of Jovian energetic auroral electrons and ultraviolet emissions by the Juno Spacecraft. *Journal of Geophysical Research: Space Physics*, *124*(11), 8298–8317. https://doi.org/10.1029/2019JA026862

Gershman, D., Connerney, J., Kotsiaros, S., DiBraccio, G., Martos, Y., Viñas, A., et al. (2019). Alfvénic fluctuations associated with Jupiter's auroral emissions. *Geophysical Research Letters*, *46*, 7157–7165. https://doi.org/10.1029/2019GL082951

Gladstone, G., Persyn, S., Eterno, J., Walther, B., Slater, D., Davis, M., et al. (2017). The Ultraviolet Spectrograph on NASA's Juno Mission. *Space Science Reviews*, *213*, 447–473. https://doi.org/10.1007/s11214-014-0040-z

Goldstein, B., Smith, E., Balogh, A., Horbury, T., Goldstein, M., & Roberts, D. (1995). Properties of magnetohydrodynamic turbulence in the solar wind as observed by Ulysses at high heliographic latitudes. *Geophysical Research Letters*, *22*(23), 3393–3396. https://doi.org/10.1029/95GL03183

Gustin, J., Gérard, J.-C., Grodent, D., Cowley, S., Clarke, J., & Grard, A. (2004). Energy-flux relationship in the FUV Jovian aurora deduced from HST-STIS spectral observations. *Journal of Geophysical Research: Space Physics*, *109*(A10). https://doi.org/10.1029/2003JA010365

Gustin, J., Grodent, D., Ray, L., Bonfond, B., Bunce, E., Nichols, J., & Ozak, N. (2016). Characteristics of north Jovian aurora from STIS FUV spectral images. *Icarus*, *268*, 215–241. https://doi.org/10.1016/j.icarus.2015.12.048

Hess, S., Delamere, P., Dolls, V., Bonfond, B., & Swift, D. (2010). Power transmission and particle acceleration along the Io flux tube. *Journal of Geophysical Research*, *115*. https://doi.org/10.1029/2009JA014928

Hill, T. (1979). Inertial limit on corotation. *Journal of Geophysical Research*, *84*, 6554. https://doi.org/10.1029/JA084iA11p06554

Jiménez, J. (2006). Intermittency in turbulence. *Physics*, 144–151. https://doi.org/10.1016/B0-12-512666-2/00368-0

Khurana, K. (2001). Influence of solar wind on Jupiter's magnetosphere deduced from currents in the equatorial plane. *Journal of Geophysical Research*, *106*, 25999–26016. https://doi.org/10.1029/2000JA000352

Knight, S. (1973). Parallel electric fields. *Planetary and Space Science*, *21*(5), 741–750. https://doi.org/10.1016/0032-0633(73)90093-7

Kurth, W., Hospodarsky, G., Kirchner, D., Mokrzycki, B., Averkamp, T., Robison, W., et al. (2017). The juno waves investigation. *Space Science Reviews*, *213*, 347–392. https://doi.org/10.1007/s11214-017-0396-y

Leamon, R., Smith, C., Ness, N., & Wong, H. K. (1999). Dissipation range dynamics: Kinetic Alfvén waves and the importance of β_e. *Journal of Geophysical Research*, *104*(A10), 22331–22344. https://doi.org/10.1029/1999ja900158

Lorch, C., Ray, L., Arridge, C., Khurana, K., Martin, C., & Bader, A. (2020). Local time asymmetries in Jupiter's magnetodisc currents. *Journal of Geophysical Research: Space Physics*, *125*. https://doi.org/10.1029/2019JA027455

Louis, C., Prangé, R., Lamy, L., Zarka, P., Imai, M., Kurth, W., & Connerney, J. (2019). Jovian auroral radio sources detected in situ by juno/waves: Comparisons with model auroral ovals and simultaneous HST FUV images. *Geophysical Research Letters*, *46*, 11606–11614. https://doi.org/10.1029/2019GL084799

Lysak, R., & Lotko, W. (1996). On the kinetic dispersion relation for shear Alfvén waves. *Journal of Geophysical Research*, *101*(5085), 5085–5094. https://doi.org/10.1029/95JA03712

Mauk, B., Clark, G., Gladstone, G., Kotsiaros, S., Adriani, A., Allegrini, F., et al. (2020). Energetic particles and acceleration regions over Jupiter's polar cap and main aurora: A broad overview. *Journal of Geophysical Research: Space Physics*, *125*. https://doi.org/10.1029/2019JA027699

Mauk, B., Haggerty, C., ParanicasClark, G., Kollmann, P., Rymer, A., Mitchell, D. G., et al. (2017). Juno observations of energetic charged particles over Jupiter's polar regions: Analysis of mono- and bi-directional electron beams. *Geophysical Research Letters*, *44*(10), 4410–4418. https://doi.org/10.1002/2016GL072286

Mauk, B., Haggerty, D., Paranicas, C., Clark, G., Kollmann, P., Rymer, A., et al. (2018). Diverse electron and ion acceleration characteristics observed over Jupiter's main aurora. *Geophysical Research Letters*, *45*, 1277–1285. https://doi.org/10.1002/2017GL076901

McComas, D., Alexander, N., Allegrini, F., Bagenal, F., Beebe, C., Clark, G., et al. (2017). The Jovian Auroral Disrtibutions Experiment (JADE) on the Juno Mission to Jupiter. *Space Science Reviews*, *213*, 547–643. https://doi.org/10.1007/s11214-013-9990-9

Meyrand, R., Kiyani, K., & Galtier, S. (2015). Weak magnetohydrodynamic turbulence and intermittency. *Journal of Fluid Mechanics*, *770*(R1). https://doi.org/10.1017/jfm.2015.141

Ng, C., Delamere, P., Kaminker, V., & Damiano, P. (2018). Radial transport and plasma heating in Jupiter's magnetodisc. *Journal of Geophysical Research: Space Physics*, *123*, 6611–6620. https://doi.org/10.1029/2018JA025345

Prêle, D. (2017). *Advanced Electronic Systems*, (p.39). cel-00843641v6.

Radioti, A., Gérard, J.-C., Grodent, D., Bonfond, B., Krupp, N., & Woch, J. (2008). Discontinuity in Jupiter's main auroral oval. *Journal of Geophysical Research*, *113*. https://doi.org/10.1029/2007JA012610

Ray, L., Su, Y.-J., Ergun, R., Delamere, P., & Bagenal, F. (2009). Current-voltage relation of a centrifugally confined plasma. *Journal of Geophysical Research*, *114*(A4). https://doi.org/10.1029/2008JA013969

Saur, J. (2004). Turbulent heating of Jupiter's middle magnetosphere. *The Astrophysical Journal*, *602*, 137–L140. https://doi.org/10.1086/382588

Saur, J., Janser, S., Schreiner, A., Clark, G., Mauk, B., Kollmann, P., et al. (2018). Wave-particle interactions of alfvén waves in Jupiter's Magnetosphere: Auroral and magnetospheric particle acceleration. *Journal of Geophysical Research: Space Physics*, *123*, 9560–9573. https://doi.org/10.1029/2018JA025948

Saur, J., Politano, H., Pouquet, A., & Matthaeus, W. (2002). Evidence for weak MHD turbulence in the middle magnetosphere of Jupiter. *Astronomy & Astrophysics*, *386*, 699–708. https://doi.org/10.1051/0004-6361:20020305

Saur, J., Pouquet, A., & Matthaeus, W. (2003). An acceleration mechanism for the generation of the main auroral oval on Jupiter. *Geophysical Research Letters*, *30*(5). https://doi.org/10.1029/2002GL015761

Tao, C., Kimura, T., Badman, S., André, N., Tsuchiya, F., Murakami, G., et al. (2016). Variations of Jupiter's aurora observed by Hisaki/EXCEED: 2. Estimations of auroral parameters and magnetospheric dynamics. *Journal of Geophysical Research: Space Physics*, *121*, 4055–4071. https://doi.org/10.1002/2015JA021272

Tao, C., Sahraoui, F., Fontaine, D., de Patoul, J., Chust, T., Kasahara, S., & Retino, A. (2015). Properties of Jupiter's magnetospheric turbulence observed by the Galileo spacecraft. *Journal of Geophysical Research: Space Physics*, *120*(4), 2477–2493. https://doi.org/10.1002/2014JA020749

Veltri, P. (1999). MHD turbulence in the solar wind: Self-similarity, intermittency and coherent structures. *Plasma Physics and Controlled Fusion*, *41*(A787), A787–A795. https://doi.org/10.1088/0741-3335/41/3A/071

von Papen, M., Saur, J., & Alexandrova, O. (2014). Turbulent magnetic field fluctuations in Saturn's magnetosphere. *Journal of Geophysical Research: Space Physics*, *119*(4), 2797–2818. https://doi.org/10.1002/2013JA019542

Wahlund, J.-E. (2003). Observations of auroral broadband emissions by Cluster. *Geophysical Research Letters*, *30*(1535). https://doi.org/10.1029/2002GL016335

Watt, C., Rankin, R., Rae, I., & Wright, D. (2005). Self-consistent electron acceleration due to inertial Alfvén wave pulses. *Journal of Geophysical Research: Space Physics*, *110*. https://doi.org/10.1029/2004JA010877

Watt, C., Rankin, R., Rae, I., & Wright, D. (2006). Inertial Alfvén waves and acceleration of electrons in nonuniform magnetic fields. *Geophysical Research Letters*, *33*. https://doi.org/10.1029/2005GL024779